## ARTICLE

# Bmi1 limits dilated cardiomyopathy and heart failure by inhibiting cardiac senescence

I. Gonzalez-Valdes[1], I. Hidalgo[1], A. Bujarrabal[1], E. Lara-Pezzi[2], L. Padron-Barthe[2,3], P. Garcia-Pavia[3], Pablo Gómez-del Arco[4,5], J.M. Redondo[4], J.M. Ruiz-Cabello[6], L.J. Jimenez-Borreguero[6], J.A. Enriquez[7], J.L. de la Pompa[8], A. Hidalgo[9] & S. Gonzalez[1]

Dilated cardiomyopathy (DCM) is the most frequent cause of heart failure and the leading indication for heart transplantation. Here we show that epigenetic regulator and central transcriptional instructor in adult stem cells, Bmi1, protects against DCM by repressing cardiac senescence. Cardiac-specific Bmi1 deletion induces the development of DCM, which progresses to lung congestion and heart failure. In contrast, Bmi1 overexpression in the heart protects from hypertrophic stimuli. Transcriptome analysis of mouse and human DCM samples indicates that p16$^{INK4a}$ derepression, accompanied by a senescence-associated secretory phenotype (SASP), is linked to severely impaired ventricular dimensions and contractility. Genetic reduction of p16$^{INK4a}$ levels reverses the pathology of Bmi1-deficient hearts. In parabiosis assays, the paracrine senescence response underlying the DCM phenotype does not transmit to healthy mice. As senescence is implicated in tissue repair and the loss of regenerative potential in aging tissues, these findings suggest a source for cardiac rejuvenation.

[1] Stem Cell Aging Group, Centro Nacional de Investigaciones Cardiovasculares (CNIC), E-28029 Madrid, Spain. [2] Molecular Regulation of Heart Development and Disease Group, Centro Nacional de Investigaciones Cardiovasculares (CNIC), E-28029 Madrid, Spain. [3] Heart Failure and Inherited Cardiac Diseases Unit, Hospital Universitario Puerta de Hierro Majadahonda, Manuel de Falla, 1, E-28222 Madrid, Spain. [4] Gene Regulation in Cardiovascular Remodelling and Inflammation Group, Centro Nacional de Investigaciones Cardiovasculares (CNIC, E-28029) Madrid, Spain. [5] Department of Molecular Biology, Universidad Autonoma de Madrid, E-28049 Madrid, Spain. [6] Advanced Imaging Unit, Ciber de Enfermedades respiratorias and UCM, Centro Nacional de Investigaciones Cardiovasculares (CNIC), E-28029 Madrid, Spain. [7] Functional Genetics of the Oxidative Phosphorylation System, Centro Nacional de Investigaciones Cardiovasculares (CNIC), E-28029 Madrid, Spain. [8] Intercellular Signaling In Cardiovascular Development and Disease Group, Centro Nacional de Investigaciones Cardiovasculares (CNIC), E-28029 Madrid, Spain. [9] Imaging the Cardiovascular Inflammation and the Immune Response, Centro Nacional de Investigaciones Cardiovasculares (CNIC), E-28029 Madrid, Spain. Correspondence and requests for materials should be addressed to S.G. (email: sgonzalez@cnic.es).

D ilated cardiomyopathy (DCM) is the commonest form of non-ischaemic cardiomyopathy and can lead to sudden cardiac death and heart failure[1]. The health burden associated with DCM is a major contribution to health-care costs; however, the mechanisms underlying the regulation of noninherited DCM remain unexplored[2]. DCM is defined by the presence of dilated and poorly functioning left ventricle in the absence of abnormal loading conditions, such as valve defect or hypertension or ischaemic heart failure sufficient to induce global systolic impairment. A large number of cardiac and systemic diseases can cause systolic impairment and left ventricular dilatation; however, in the majority of patients no identifiable cause is found (hence, idiopathic DCM). Therefore, understanding the aetiology of idiopathic DCM is of great clinical relevance in view of the devastating consequences of this disease in a large patient population.

The epigenetic signature establishes a cell-type-specific chromatin pattern that is of paramount importance for cell commitment and regeneration during development and adulthood[3–5]. Epigenetic regulation offers a critical means for governing cardiac gene expression under different physiological and pathological states[6]. In fact, the nature of cardiomyopathy and heart failure intensely links with irregular cardiac gene expression. One of the causes of congenital heart disease is deficiency for specific epigenetic instructors during cardiogenesis[5], such as the histone methyltransferases *Ezh2* (ref. 7) and *MLL2* (ref. 8), or transcription factors *Tbx5* and *Nkx2-5* that require histone-modifying enzymes to regulate gene expression[5]. Essential epigenetic changes at developmental cardiac-specific genes are also required for reprogramming of cardiac fibroblasts (FBs) into cardiomyocytes (CMs) and for cardiac lineage commitment[9,10]. However, the role of critical epigenetic modifications in adult cardiac function has received comparatively little attention. A good example of that is the well-established role of epigenetic Bmi1 factor in the maintenance of adult stem cell populations[11]; however, its direct or indirect implication in regulating the cardiac function is unknown.

Senescence protects organisms against damaged cells by inducing a stable growth arrest not only in tumour suppression[12] but also in noncancer pathologies[13]. Growth arrest is achieved, at least in part, through activation of the p16[INK4a]/Retinoblastoma tumour-suppressor pathways[14,15]. Concomitant with this arrest, senescent cells communicate with their environment, secreting a complex mixture of factors called the senescence-associated secretory phenotype (SASP) or senescence-messaging secretome[16,17].

Here we reasoned that the epigenetic factor Bmi1 might be involved in the maintenance of adult cardiac function. Using a combination of conditional knockout models, biochemical analysis, parabiotic assays and characterization of the DCM transcriptional signature in humans and mice, this study reveals the importance of a genuinely protective role of the epigenetic Bmi1 in cardiac adult pathophysiology, namely protection of adult heart from cellular senescence. Therefore, controlling cardiac gene expression by epigenetic-regulating factors gives a promising approach to the treatment of human cardiomyopathy.

## Results

**Bmi1 expression is not required for cardiogenesis.** Several epigenetic Polycomb regulators are differently regulated during embryonic development and adult aging[18], prompting us to analyse endogenous cardiac *Bmi1* expression in the mouse. The amount of Bmi1 increased progressively throughout cardiogenesis, stabilizing in adulthood, and then declining in the hearts of aged mice (Supplementary Fig. 1a). This profile correlated inversely with the levels of p16[INK4a] (Supplementary Fig. 1b), as noted in other studies with adult stem cells[19–24]. To analyse the implication of Bmi1 in heart failure, we induced hypertrophy in wild-type mouse hearts, either surgically with a transverse aortic constriction (TAC) or by infusion with isoproterenol (Supplementary Fig. 1c). We additionally analysed the left ventricular myocardium from eight non-failing and eight failing human hearts. In humans and mice, analysis of cardiac Bmi1 expression showed a marked reduction in failing hearts, levels inversely correlated with *p16[INK4a]* expression (Supplementary Fig. 1c,d). These results indicate a possible association of Bmi1 downregulation with the development of cardiac hypertrophy.

To explore the implication of Bmi1 in cardiogenesis, we crossed *Bmi1^{fl/fl}* mice with *Nkx2.5-Cre[tg/+]* mice[25] to induce cardiac-specific *Bmi1* deletion from embryonic day (E) 7.5 onwards. *Bmi1[f/f];Nkx-Cre[tg/+]* mice were born at normal Mendelian frequency and were able to support pregnancy. Histologic examination of *Bmi1[f/f];Nkx-Cre[tg/+]* embryos at E14.5 − E18.5 did not reveal any cardiac abnormality (Fig. 1a). Expression of *Bmi1* mRNA on post-natal day 2 (P2) was significantly lower in *Bmi1[f/f];Nkx-Cre[tg/+]* hearts than in controls and correlated with below-normal levels of the epigenetic mark H3K9me3 (Fig. 1b; Supplementary Fig. 1e). Interestingly, *Bmi1[f/f]; Nkx-Cre[tg/+]* hearts also had a significantly higher heart-to-body-weight (HW/BW) ratio, and expressed higher levels of fetal cardiac genes than littermate controls (Fig. 1c; Supplementary Fig. 1f). Histological comparison with *Bmi1[f/f];Nkx-Cre^{+/+}* controls at 22 weeks after birth showed that *Bmi1*-null hearts were enlarged and presented fibrosis and CMs with the above-normal cross-sectional area (Fig. 1d; Supplementary Fig. 1g). Two-dimensional echocardiography revealed the hearts of *Bmi1[f/f];Nkx-Cre[tg/+]* mice to be dilated and poorly contractile (Fig. 1e). These hearts, moreover, had a markedly enlarged left ventricular internal diameter at diastole and severely depressed left ventricular mass and fractional shortening, a direct measure of cardiac contractile function, consistent with progressive DCM (Fig. 1e,f). Lung weight in 22-week-old *Bmi1[f/f];Nkx-Cre[tg/+]* mice was significantly increased (Fig. 1g; Supplementary Fig. 1h), suggesting the development of lung oedema secondary to the LV dysfunction. This was confirmed by serial pulmonary magnetic resonance imaging (MRI), which revealed significant pulmonary congestion and oedema (Fig. 1h) coinciding with the impaired cardiac contractile function and maximal left ventricular dilatation for Bmi1-null hearts (Fig. 1f). Perl's Prussian blue staining on lung sections revealed impaired permeability of the alveolar septal barrier in *Bmi1[f/f];Nkx-Cre[tg/+]* mice, indicated by the accumulation of siderophages (hemosiderin-laden macrophages) in the perivascular regions of *Bmi1[f/f];Nkx-Cre[tg/+]* lungs (Fig. 1i). All *Bmi1[f/f];Nkx-Cre[tg/+]* mice died between 20 and 30 weeks, whereas *Bmi1[f/f]; Nkx-Cre^{+/+}* had a normal lifespan (Fig. 1j). These data thus suggest that cardiac *Bmi1* deletion during embryogenesis does not affect cardiogenesis but causes DCM in adulthood.

**Adult Bmi1 deficiency causes DCM.** To further test the contribution of *Bmi1* deficiency to heart disease, we engineered CM-specific *Bmi1* deletion in adulthood by crossing *Bmi1^{fl/fl}* mice[24] with the α-myosin heavy chain (αMHC)-Cre[tg/+] strain[26]. Conditional mutants occurred at a normal Mendelian ratio, indicating an absence of embryonic lethality. Examination of 5-week-old *Bmi1[f/f];αMHC-Cre[tg/+]* mice confirmed cardiac *Bmi1* deletion (Supplementary Fig. 2a). At 12 weeks of age, *Bmi1[f/f]; αMHC-Cre[tg/+]* mice showed typical features of DCM: impaired cardiac ejection fraction, a high HW/BW ratio, enlarged CMs,
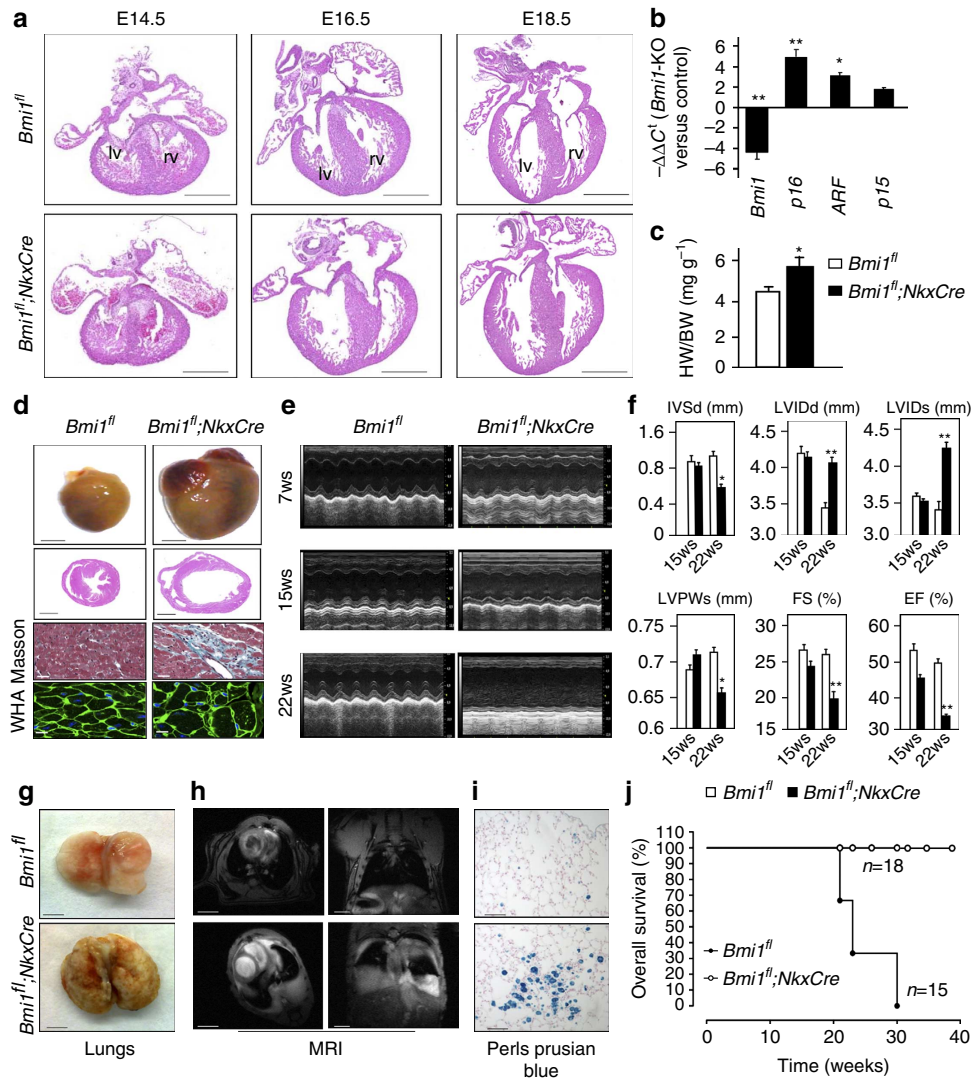
**Figure 1 | Bmi1 is not required for normal cardiac development.** (**a**) Representative heart sections from $Bmi1^{f/f};Nkx\text{-}Cre^{tg/+}$ ($Bmi1^{fl};NkxCre$) and $Bmi1^{f/f};$ $Nkx\text{-}Cre^{+/+}$ ($Bmi1^{f/}$) E14.5, E16.5 and E18.5 embryos (scale bar, 200 μm). Rv, right ventricle; lv, left ventricle. (**b**) Quantitative RT–PCR (qRT–PCR) analysis of $Bmi1$, $p16^{INK4a}$, $ARF$ and $p15^{INK4b}$ mRNA expression in total heart cells from $Bmi1^{fl};NkxCre$ (Bmi1-knock out) mice. Data are standardized to β-actin levels and are expressed relative to $Bmi1^{f/}$ (Control) mice (means ± s.d.; $n = 12$, *$P < 0.05$; Student's $t$-test). (**c**) HW/BW ratio in 22-week-old $Bmi1^{fl};NkxCre$ mice and $Bmi1^{f/}$ controls (means ± s.d.; $n = 12$, *$P < 0.05$; Student's $t$-test). (**d**) Gross cardiac phenotype of 22-week-old $Bmi1^{fl};NkxCre$ mice and $Bmi1^{f/}$ controls. Representative views are shown of external anatomy (top row; bars, 0.5 cm) and haematoxylin and eosin (H&E) staining on sections in adult hearts (second row; bars, 1 mm), Masson's trichrome staining to detect fibrosis (third row; bars, 40 μm) and left ventricular muscle sections stained with wheatgerm agglutinin (WGA; bottom row; bars, 10 μm). (**e,f**) *Trans*-thoracic M-mode echocardiographic and physiological analyses of $Bmi1^{fl};NkxCre$ and $Bmi1^{f/}$ mice. Panel **i** shows representative traces from $Bmi1^{fl};NkxCre$ and $Bmi1^{f/}$ mice at 7, 15 and 22 weeks of age. IVSd, diastolic interventricular septal wall thickness; LVDd, diastolic left ventricular internal dimension; LVDs, systolic left ventricular internal dimension; LVPWd, diastolic left ventricular posterior wall thickness; FS, fractional shortening of left ventricle dimension; EF, ejection fraction; LVmass, left ventricular mass. Data are means ± s.d. ($n = 12$, **$P < 0.001$, *$P < 0.05$; Student's $t$-test). (**g**) Representative images of whole lungs from 12-week-old $Bmi1^{fl};NkxCre$ mice and $Bmi1^{f/}$ littermates. Scale bars, 5 mm. (**h**) Thoracic magnetic resonance MRI of similar mice in transverse view, showing both heart and lungs (left), and in the coronal view (right). Scale bars, 2.5 mm. (**i**) Representative Perls iron staining of lung sections from mice as in **g**, **h** (bars, 30 μm). (**j**) Kaplan–Meier survival curve for $Bmi1^{fl};NkxCre$ mice and $Bmi1^{f/}$ littermates (means ± s.d., $P < 0.001$; Student's $t$-test).

fibrosis and larger-than-normal ventricular chambers (Fig. 2a,b; Supplementary Fig. 2b). These cardiac defects were accompanied by pulmonary oedema and the presence of siderophages (Fig. 2c–e). Consistent with this phenotype, adult $Bmi1^{f/f};$ $\alpha MHC\text{-}Cre^{tg/+}$ mice developed full-blown DCM and suffered heart failure at 15–20 weeks of age (Fig. 3f).

To test whether heart failure was sensitive to the Bmi1 dosage, we analysed the hearts of $Bmi^{fl/+};\alpha MHC\text{-}Cre^{tg/+}$ and $Bmi^{fl/+};$ $\alpha MHC\text{-}Cre^{+/+}$ mice. Young $Bmi1$ heterozygotes showed no noticeable cardiac defects (Supplementary Fig. 2c); however, at

∼6 months, they developed characteristics of DCM, including a severely depressed ejection fraction (Supplementary Fig. 2c), a trend towards a high HW/BW ratio (Supplementary Fig. 2d) and interstitial fibrosis (Supplementary Fig. 2e). These mice invariably died by 7 months after birth (Supplementary Fig. 2f), indicating that Bmi1 is critical to maintain adult heart function.

To confirm the requirement of Bmi1 in the adult heart, we used a tamoxifen (TM)-inducible α-myosin heavy chain $(\alpha MHC)^{TM}\text{-}Cre$ line[27] to delete $Bmi1$ in the hearts of 5-week-old adult mice (Fig. 3a,b). Heart weight and function in
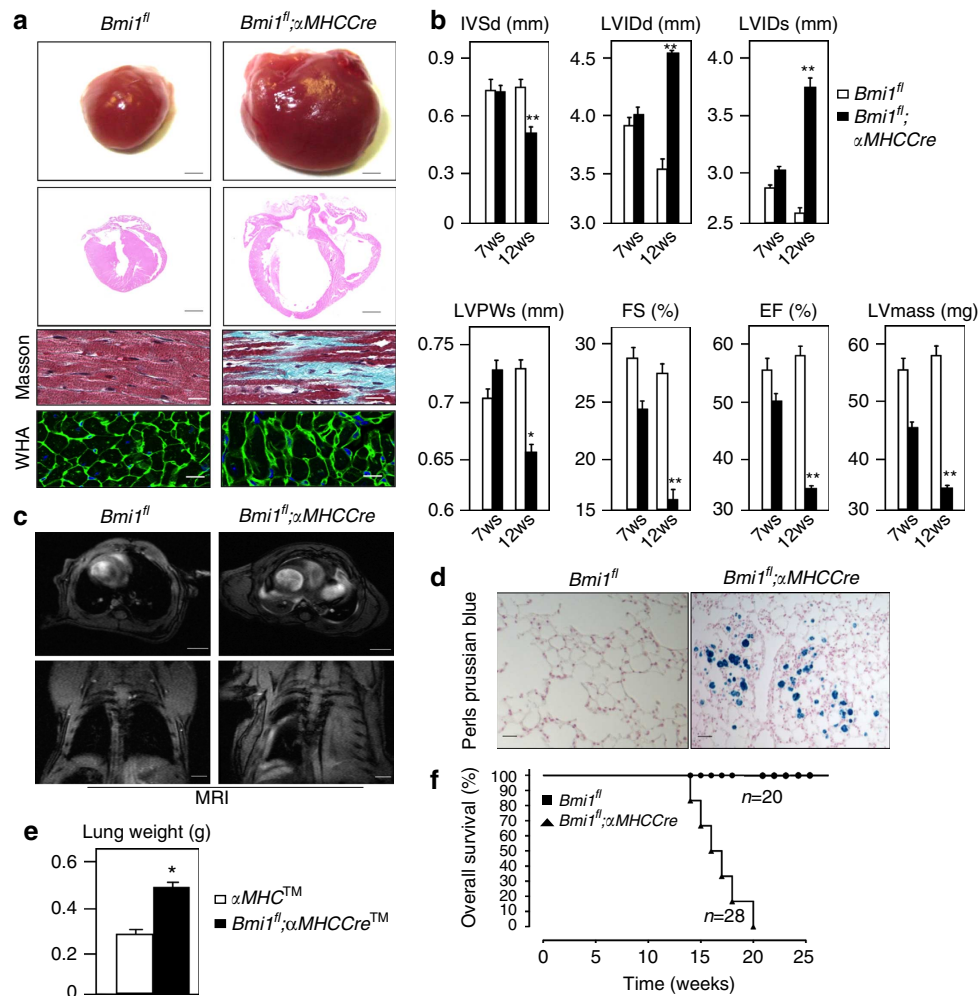
**Figure 2 | Bmi1 activation blocks development of cardiac hypertrophy.** (**a**) Gross cardiac phenotype of *Bmi1^fl^;αMHCCre* mice and *Bmi1^fl^* controls. Representative views are shown of external anatomy and H&E staining on sections in adult hearts (12-week-old; top two rows; bars, 50 mm), Masson's trichrome staining to detect fibrosis (third row; bars, 40 μm) and left ventricular muscle sections stained with WGA to detect cardiomyocyte borders (bottom row; bars, 10 μm). (**b**) M-mode echocardiographic analysis of *Bmi1^fl^;αMHCCre* and *Bmi1^fl^* mice. IVSd, diastolic interventricular septal wall thickness; LVDd, diastolic left ventricular internal dimension; LVDs, systolic left ventricular internal dimension; LVPWd, diastolic left ventricular posterior wall thickness; FS, fractional shortening of left ventricle dimension; EF, ejection fraction; LVmass, left ventricular mass. Data are means ± s.d. ($n = 13$, **$P < 0.001$, *$P < 0.05$; Student's $t$-test). (**c**) Thoracic MRI of *Bmi1^fl^;αMHCCre* and *Bmi1^fl^* mice in transverse view, showing both heart and lungs (top), and in coronal view (bottom). Scale bars, 2.5 mm. (**d**) Representative Perls iron staining of lung sections from representative 12-week-old *Bmi1^fl^;αMHCCre* and *Bmi1^fl^* littermates (bars, 30 μm). (**e**) Lung weight in 12-week-old *Bmi1^f/f^;αMHC^TM^-Cre^tg/+^* and *Bmi1^+/+^;αMHC^TM^-Cre^tg/+^* mice (means ± s.d.; $n = 10$, *$P < 0.05$; Student's $t$-test). (**f**) Kaplan–Meier survival curve for *Bmi1^fl^;αMHCCre* mice and *Bmi1^fl^* littermates (means ± s.d.**$P < 0.001$; Student's $t$-test).

*Bmi1^f/f^;αMHC^TM^-Cre^tg/+^* conditional knockouts and *Bmi1^f/f^; αMHC^TM^-Cre^+/+^* and *Bmi1^+/+^;αMHC^TM^-Cre^tg/+^* control mice were monitored using histology and echocardiography (Fig. 3c–e). At 12 weeks post-TM treatment, average left ventricular internal diameter at diastole was similar in control and conditional knockout mice; however, dilatation and loss of contractility subsequently became evident in the mutants (Fig. 3d,e). At 22 weeks post induction, ventricular diameter in *Bmi1^f/f^;αMHC^TM^-Cre^tg/+^* mice had increased from 3.8 mm at baseline to 4.59 mm, correlating with a fractional shortening of 17% (Fig. 3d,e). MRI revealed significant pulmonary congestion and oedema, which correlated with a 54% increase in lung weight, compared with TM-treated control littermates (Fig. 3f,g). Iron overload in the lung, detected by Perl's staining, was also evident (Fig. 3h). TM-treated *Bmi1^f/f^;αMHC^TM^-Cre^tg/+^* mice died between 28 and 32 weeks (23 and 27 weeks post induction), compared with only 1% of TM-treated control littermates

(Fig. 3i). Thus, Bmi1 regulates CM function and maintenance throughout adult life.

**Bmi1 overexpression in the heart safeguarded the hypertrophic stage.** To assess the antihypertrophic effect of Bmi1, we crossed the doxycycline-inducible *MLC2-rRTA^tg/+^* mouse line[28] with *tetO-Bmi1^tg/tg^* mice, generating *iBmi1^tg/tg^;MLC2^tg/+^* mice and *iBmi1^tg/tg^;MLC2^+/+^* control littermates (hereafter *iBmi1^tg^;MLC2* and *iBmi^tg^* control mice). Inclusion of doxycycline in the drinking water of 8-week-old *iBmi1^tg/tg^;MLC2^tg/+^* mice induced cardiac-specific overexpression of Bmi1 (Fig. 4a; Supplementary Fig. 3a). Doxycycline treatment did not induce overt cardiac abnormalities in *Bmi1* transgenic mice or control counterparts (Fig. 4b–d). As in wild-type mice, TAC surgery in doxycycline-treated *iBmi1^tg/tg^;MLC2^+/+^* controls triggered massive cardiac hypertrophy, an increase in CM cross-sectional area and fibrosis (Fig. 4b–e;

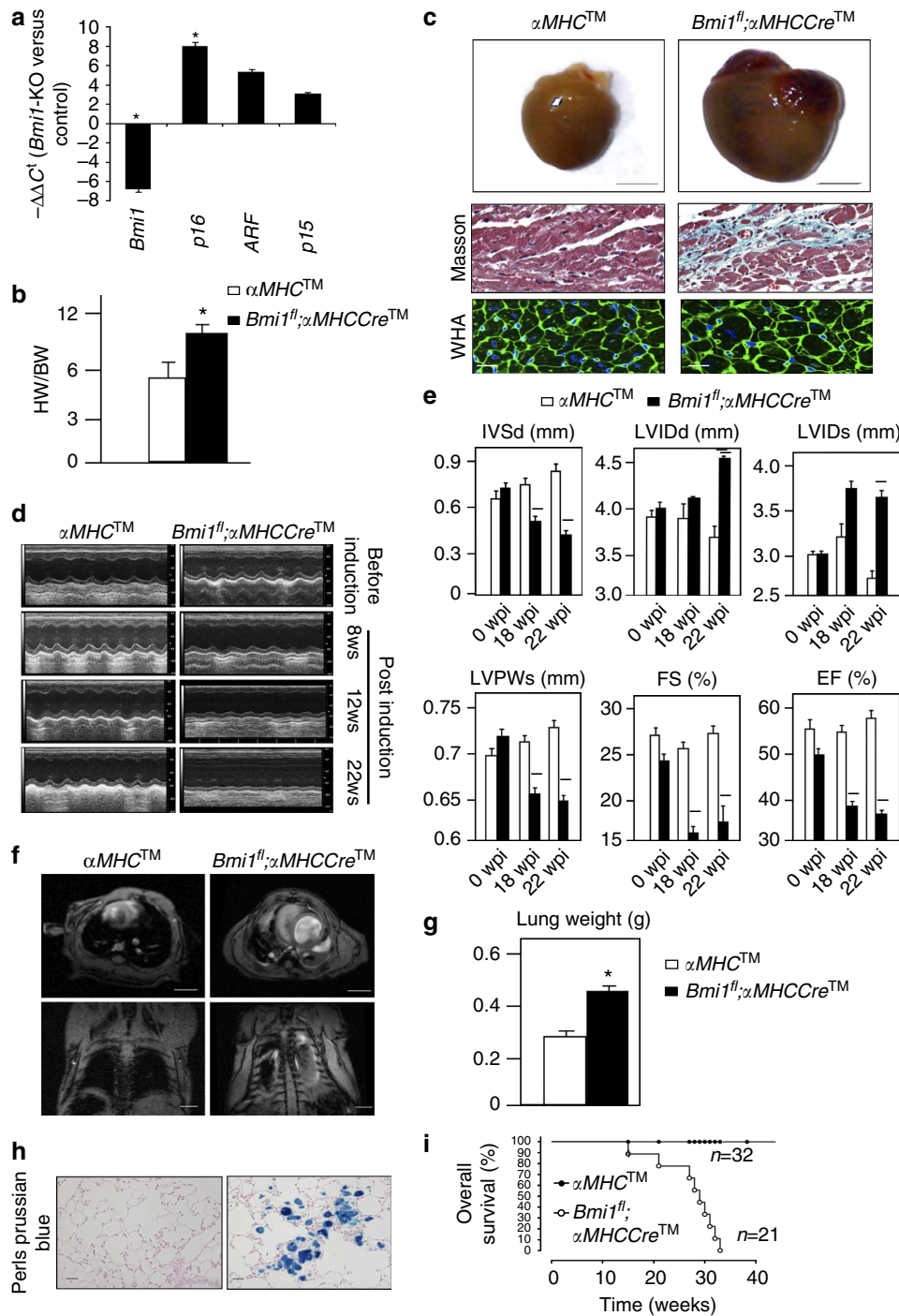**Figure 3 | Cardiac dysfunction in tamoxifen-treated *Bmi1^{f/f};αMHC^{TM}-Cre^{tg/+}* mice.** (**a**) qRT–PCR analysis of the mRNA expression of *Bmi1*, *p16^{INK4a}*, *ARF* and *p15^{INKb}* in total heart cells from *Bmi1^{fl};αMHCCre^{TM}* (Bmi1-KO) and *αMHCCre^{TM}* (Control) mice. Data are standardized to β-actin levels and are expressed relative to Control mice (means ± s.d.; n = 9, *P < 0.05; Student's t-test). (**b**) HW/BW ratio in *Bmi1^{fl};αMHCCre^{TM}* mice and *αMHCCre^{TM}* controls mice at 22 weeks post induction (27 weeks old; means ± s.d.; n = 10, *P < 0.05; Student's t-test). (**c**) Gross cardiac phenotype of *Bmi1^{fl};αMHCCre^{TM}* mice and *αMHCCre^{TM}* controls at 22 weeks post induction (27 weeks old). Representative views are shown of external anatomy (bar, 50 mm), Masson's trichrome staining to detect fibrosis (bars, 40 μm), left ventricular muscle sections stained with WGA to detect cardiomyocyte borders (bars, 10 μm). (**d,e**) *Trans*-thoracic M-mode echocardiographic and physiological analyses of *Bmi1^{fl};αMHCCre^{TM}* and *αMHCCre^{TM}* mice at 8, 12 and 22 weeks post induction. Panel **e** shows representative traces. Panel **g** shows echocardiographic measurements and physiological parameters. IVSd, diastolic interventricle septal wall thickness; LVDd, diastolic left ventricle internal dimension; LVDs, systolic left ventricle internal dimension; LVPWd, diastolic left ventricle posterior wall thickness; FS, fractional shortening of left ventricle dimension; EF, ejection fraction; LVmass, left ventricle mass. Data are means ± s.d.; n = 12, **P < 0.001, *P < 0.05; Student's t-test. (**f**) Thoracic MRI of representative 12-week-old *Bmi1^{fl};αMHCCre* mice and *Bmi1^{f/f}* littermates in transverse view, showing both heart and lungs (top), and in coronal view (bottom). Scale bars, 2.5 mm. (**g**) Lung weight in *Bmi1^{fl};αMHCCre^{TM}* mice and *αMHCCre^{TM}* controls at 22 weeks post induction (27 weeks old; means ± s.d.; n = 10, *P < 0.05; Student's t-test). (**h**) Representative Perls iron staining of lung sections from representative 12-week-old *Bmi1^{fl};αMHCCre* mice and *Bmi1^{f/f}* littermates (bars, 30 μm). (**i**) Kaplan–Meier survival curve for *Bmi1^{fl};αMHCCre* mice and *Bmi1^{f/f}* littermates (means ± s.d. **P < 0.001; Student's t-test).
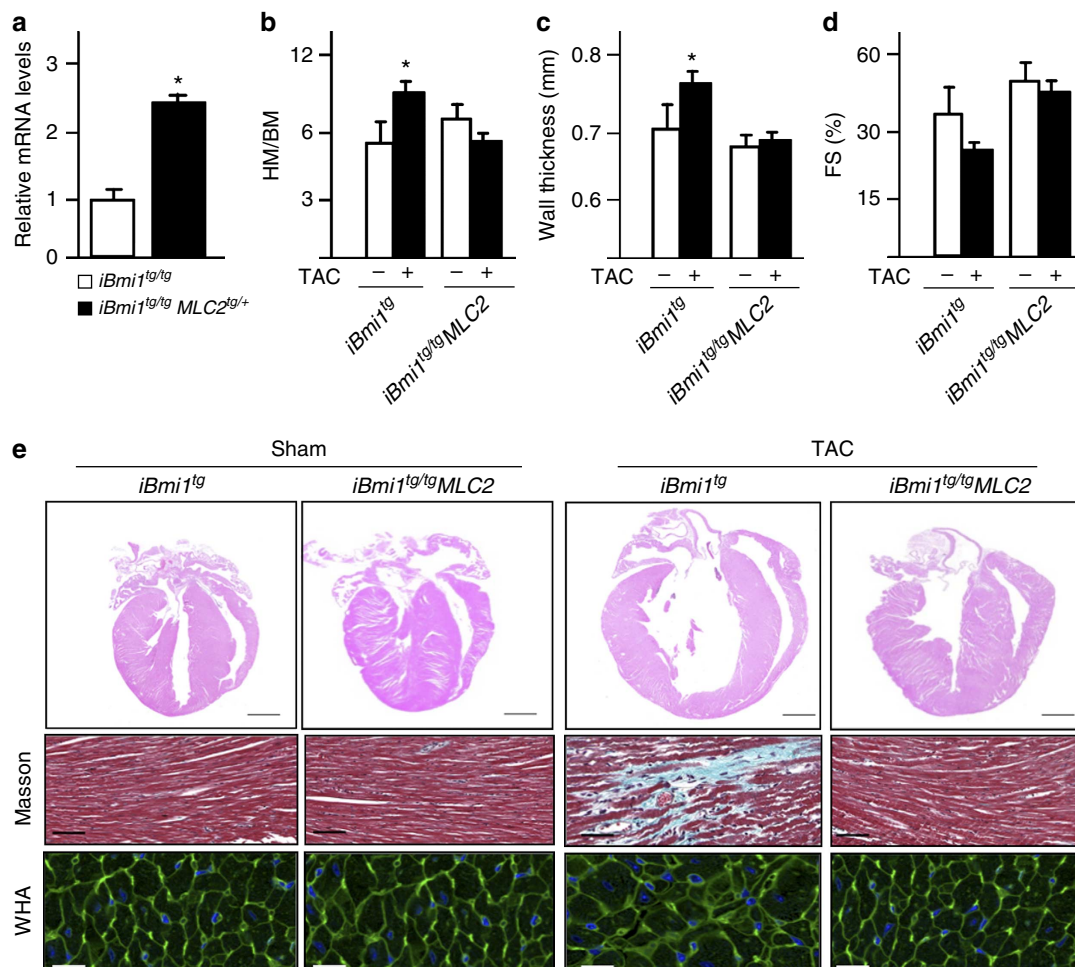
**Figure 4 | Bmi1 activation blocks development of cardiac hypertrophy.** (**a**) mRNA levels of Bmi1 in heart samples from nontransgenic control mice ($iBmi1^{tg/tg}$) and Bmi1 transgenic mice ($iBmi1^{tg/tg}$;$MLC2^{tg/+}$; means ± s.d.; $n = 8$, *$P < 0.05$; Student's $t$-test). (**b**) HW/BW ratios in $iBmi1^{tg/tg}$;$MLC2$ mice and $iBmi^{tg}$ littermates 4 weeks after the TAC surgery or sham operation. Data are means ± s.d.; $n = 8$ mice per group (means ± s.d.; $n = 6$, *$P < 0.05$; Student's $t$-test). (**c,d**) Left ventricular wall thickness and fractional shortening measured using echocardiography in the same hearts as in **b**. (**e**) Representative low-magnification views of H&E-stained cross-sections at the midventricle from nontransgenic and Bmi1 transgenic mice subjected to sham or TAC treatment and stained with WGA (top; scale bars, 10 μm) or Masson's trichrome to detect fibrosis (bottom; scale bars, 40 μm).

Supplementary Fig. 3b). In contrast, TAC surgery induced none of these symptoms in the hearts of doxycycline-treated $iBmi1^{tg/tg}$;$MLC2^{tg/+}$ mice (Fig. 4e), indicating that Bmi1 overexpression blocks pathological ventricular remodelling.

**Regulation of a cardiac-specific transcriptional programme by Bmi1.** To explore the primary cause of DCM in Bmi1-null mice, we set out to identify differentially expressed genes by massively parallel sequencing of heart samples from DCM-diagnosed patients who had undergone heart transplant (hDCM) and from $Bmi1^{f/f}$;$\alpha MHC^{TM}$-$Cre^{tg/+}$ mice (17-week post induction; mDCM). Pairwise comparisons (with corresponding controls) identified 649 and 2,435 genes differentially expressed in mDCM and hDCM samples, respectively (Fig. 5a; Supplementary Data set). Differentially upregulated genes common to mDCM and hDCM samples included those associated with the fetal cardiac gene programme[29], such as Acta2, Myh7 and Myl1 and genes encoding extracellular matrix components and regulators, such as Tgfβ, collagens, chemokines and metalloproteinases (Fig. 5a). Significantly upregulated senescence genes were the critical senescence regulator $p16^{INK4a}$ ($Cdkn2a$)[19,30,31] and essential components of the SASP (chemokines and Tgfβ family ligands;

Fig. 5a). Consistent with the proliferative arrest that accompanies senescence, we found downregulated genes related to cell-cycle progression such as CDKN3, CyclinD2 and CyclinA2 (CCNA2). There was, moreover, robust upregulation of genes encoding pro-inflammatory factors associated with the SASP, including interleukin (IL)-6, IL-7, granulocyte macrophage colony-stimulating factor and certain insulin-like growth factor-binding proteins[32]. These findings are suggestive of an important role of the senescence response mediated by the Bmi1/$p16^{INK4a}$ axis in cardiac pathophysiology, consistent with the role of Bmi1 in preventing senescence in other contexts[19].

To assess the epigenetic signature on the promoter regions of Bmi1 target genes, chromatin silencing was examined by measuring ubiquitination of histone H2A at the Lys119 residue (H2AK119ub), a histone modification mediated by PRC1 (ref. 3), and by Bmi1-specific binding using mDCM and control hearts (Fig. 5b). Additional Ezh1/Ezh2-dependent repressive H3K27me3 mark[30], and the chromatin active H3K4me3 mark were also analysed[3] (Fig. 5b). Absence of Bmi1 led to an important increase in H3K27me3 mark bound and significantly enriched for the H2AK119ub signal in the promoter regions of the downregulated CyclinA2, Gbe1 and Gmnn genes, but not in the promoters of upregulated $p16^{INK4a}$, Il1 and Tgfβ3 genes in
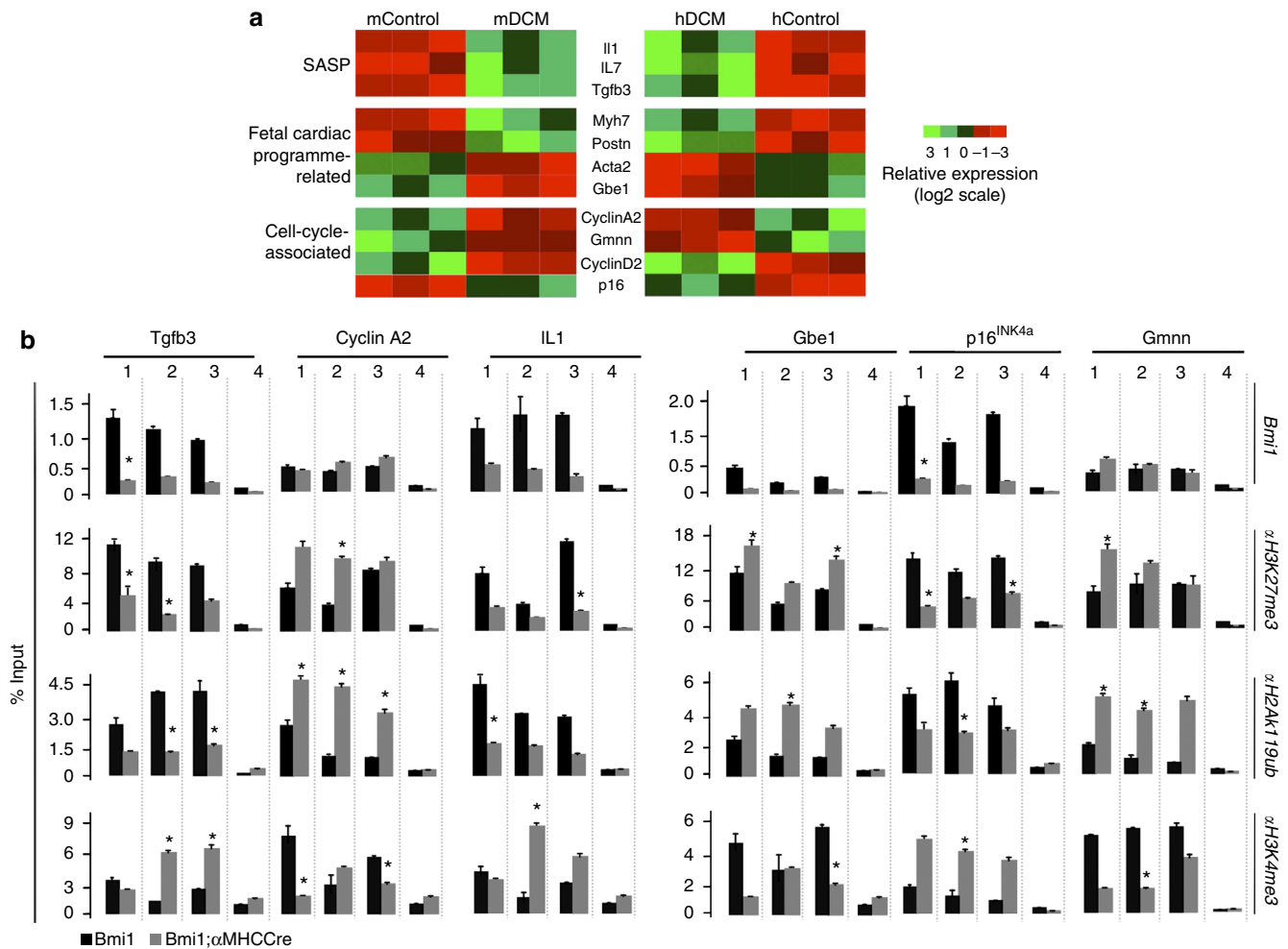
**Figure 5 | Control of cardiac-specific profile by Bmi1.** (**a**) Representative heat maps show the expression of genes with fetal cardiac programme-related genes, senescence-associated and cell-cycle functional annotations that are significantly down- and upregulated in $Bmi1^{f/f};\alpha MHC^{TM}-Cre^{tg/+}$ (mDCM) and control heart cells (mControl), and hDCM and hControl. The rows correspond to genes and the columns to samples. Gene expression values (relative to the mean expression in control cells) are indicated on a $\log_2$ scale according to a colour scheme shown. (**b**) ChIP analyses of the promoter regions in the indicated genes from total heart cells from $Bmi1^{f/f};\alpha MHC^{TM}-Cre^{tg/+}$ mice and littermate controls. Chromatin-bound DNA was probed with antibodies to Bmi1, H3K27me3, H2AK119 and H3K4me3. Percentages of input DNA are shown as the means ± s.d. of triplicate independent experiments ($*P < 0.05$; Student's $t$-test; Student's $t$-test).

$Bmi1^{f/f};\alpha MHC-Cre^{tg/+}$ hearts (Fig. 5b). However, Bmi1 binding was located at the promoters of downregulated genes in the $Bmi1^{f/f};\alpha MHC-Cre^{+/+}$ control hearts. Interestingly, mDCM heart cells showed a stronger association with H3K4me3 at the RD domain in the $p16^{INK4a}$/ARF locus, which has been demonstrated to be the main Bmi1-binding site in this locus[33,34]. In contrast, specific binding of H3K4me3 to the promoter regions of $CyclinA2$, $Gbe1$ and $Gmnn$ was lower in the absence of Bmi1 (Fig. 5b). These gene expression data strongly correlate with the cardiac phenotype of Bmi1-null mice and suggest the implication of the senescence response in the progression of DCM.

**CM senescence is increased in a Bmi1-specific manner.** Sections from 12-week-old $Bmi1^{f/f};\alpha MHC-Cre^{tg/+}$ hearts, but not controls, stained positive for senescence-associated β-galactosidase (SA-β-gal) marker (Fig. 6a). In contrast, apoptotic-mediated caspase 3 expression was not detected in $Bmi1^{f/f};\alpha MHC-Cre^{tg/+}$ or control hearts (Fig. 6a). We next assessed proliferation rate and cardiac SA-β-gal activity[35] in CMs isolated by the Langendorff

perfusion method[36] and nonmyocyte subpopulations of FBs (CD3$^-$/CD31$^-$/Thy1$^+$) and endothelial cells (ECs; CD3$^-$/CD31$^+$/Thy1$^-$)[37]. Bmi1 expression in $Bmi1^{f/f};\alpha MHC-Cre^{tg/+}$ CMs was ~10% of the level detected in control CMs, whereas FBs and ECs showed no significant differences between the two genotypes (Fig. 6b), as expected[26]. Analysis of the cell-cycle status by 5-bromodeoxyuridine (BrdU) incorporation indicated that total cardiac cells and the FB and EC subpopulations cycled similarly in mutant mice and control littermates (Fig. 6c). In $Bmi1^{fl};\alpha MHCCre$ hearts, ~31% of CMs were positive for SA-β-gal activity, compared with 18.4% in control hearts (Fig. 6d,e). Surprisingly, ~21% of FBs in $Bmi1$-null hearts were also positive, compared with 13% in control hearts (Fig. 6d,e), suggesting that CM-expressed Bmi1 might directly control the expression of paracrine factors that spread the senescence response to surrounding populations. To test this, we assessed the contribution of Tgfβ family ligands[17] to DCM in $Bmi1$-null mice. Injection of Tgfβ-neutralizing antibodies into $Bmi1^{f/f};\alpha MHC-Cre^{tg/+}$ mice significantly reduced maximum left ventricular wall thickness and reversed the fractional shortening (Supplementary Fig. 3c,d). Moreover, Tgfβ blockade significantly

reduced CM cross-sectional area (Supplementary Fig. 3e). Together, these results indicate that senescence originating in CMs plays an important role in the development of DCM in *Bmi1*-null hearts.

**Bmi1 limits the senescence response in the heart by repressing Cdkn2a.** To further define the involvement of senescence in the

DCM of cardiac Bmi1-deficient mice, we eliminated $p16^{INK4a}$ expression in the $\alpha MHCCre$-mediated *Bmi1*-null background, generating $Bmi1^{fl/fl};\alpha MHC\text{-}Cre^{tg/+};p16^{INK4a-/-}$ mice and $Bmi1^{fl/fl};\alpha MHC\text{-}Cre^{+/+};p16^{INK4a-/-}$ littermates. Deletion of $p16^{INK4a}$ ($p16^{-/-}$), with $p19ARF$ expression unaffected[38], was neither accompanied by compensatory upregulation of other Polycomb members nor by increase in p53 and p21 senescence
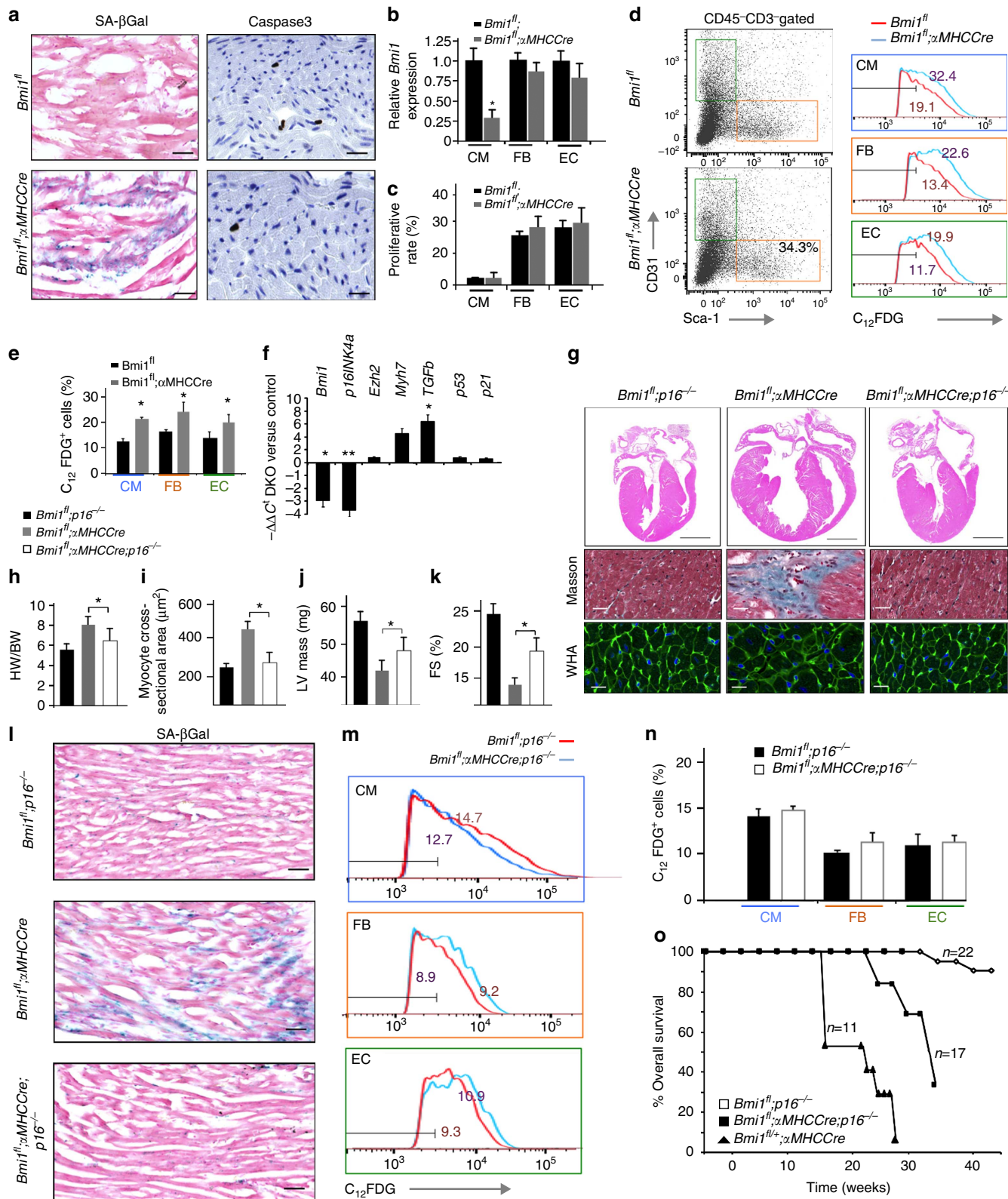
markers (Fig. 6f). Moreover, $p16^{-/-}$ mice with intact Bmi1 ($Bmi1^{fl/fl};p16^{-/-}$) showed no noticeable adult cardiac abnormalities over the period of study (40 weeks; Fig. 6g–k). $Bmi1^{fl/fl};\,\alpha MHC\text{-}Cre^{tg/+};p16^{-/-}$ mice had normal expression levels of the hypertrophy marker Myh7 and the profibrosis factor Tgfβ (Fig. 6f), and their hearts were of near normal size (Fig. 6g,h) and contained CMs of normal cross-sectional area, with no gross evidence of fibrosis (Fig. 6g,i). $Bmi1^{fl/fl};\alpha MHC\text{-}Cre^{tg/+};p16^{-/-}$ mice also had normal left ventricular wall thickness (Fig. 6j) and significantly improved FS capacity (Fig. 6k). Notably, the deletion of $p16$ almost completely averted the senescence effect of cardiac $Bmi1$ deletion, as shown by the normal proportion of CMs exhibiting SA-β-gal activity (14.4% in $Bmi1^{fl/fl};\alpha MHC\text{-}Cre^{tg/+};p16^{-/-}$ mice and 15.2% in $Bmi1^{fl/fl}p16^{-/-}$ controls; Fig. 6l–n). Moreover, $p16$ deletion significantly improved survival of mice lacking Bmi (Fig. 6n), suggesting that $p16^{INK4a}$ is required for the senescence effect in Bmi1-null hearts.

Exposure of an old mouse to the circulation of a young mouse by parabiosis can reverse major effects of age-related cardiac hypertrophy[39]. Moreover, senescent cells can communicate with their environment in a paracrine manner[17]. These observations prompted us to examine the impact of the systemic environment on senescence by surgically conjoining the circulation of $Bmi1^{f/f};\alpha MHC\text{-}Cre^{tg/+}$ and control littermate mice in parabiotic pairs (Fig. 7a). Efficiency of parabiosis was evaluated by using congenic markers to distinguish blood cells in parabiotic pairs, in which one partner was CD45.1$^+$ (Supplementary Fig. 3f). The effect of a wild-type circulation on DCM hearts (parabiotic no-DCM/DCM pairs) after 1 month was readily apparent on cardiac histologic sections (Fig. 7b). Masson's trichrome staining showed a reduction in interstitial cardiac fibrosis in the DCM heart, accompanied by reduced CM size (Fig. 7b). Accordingly, parabiosis reduced the HW/BW ratio and CM cross-sectional area in the DCM heart, whereas isochronic parabiosis (no-DCM/no-DCM or DCM/DCM pairs) had no effect (Fig. 7c,d). Parabiotic exposure of DCM mice to the circulation of healthy non-DCM littermates for 4–5 weeks rescued FS from initial values of 16.0 ± 1.1–24.0 ± 2.4% (Fig. 7e), indicating that the wild-type circulation restores cardiac function of the DCM partner in no-DCM/DCM pairs. These data indicate that factors in the circulation could modify discrete molecular pathways associated with ventricular remodelling and DCM, allowing reversal of the dilated cardiac function. Remarkably, however, DCM-related paracrine senescence factors were not able to transmit the DCM phenotype to healthy mice.

## Discussion

Here we propose a mechanistic model of how Bmi1 protects from DCM by limiting heart senescence. Absence of cardiac $Bmi1$ profoundly compromises expression of the senescence marker $p16^{INK4a}$ in CMs, leading to a cardiac-senescent response caused likely by SASP, which mobilizes the systemic and local tissue milieu for tissue repair and aging[12,40]. The detection of senescence factors by neighbouring healthy cells might further drive cellular senescence, thus contributing to a spiral of increasing inflammation and dysfunction that increases the original features of the DCM. The increasing burden of senescent cells might contribute to the early aetiology of DCM and accelerate progression of these age-related cardiac diseases (Fig. 8a). Remarkably, this paracrine nonproliferative senescence phenotype is not propagated between organisms via parabiosis, whereas a healthy circulation is able to reverse CM hypertrophy in mice with DCM. This effect is gender-independent and the reduction in CM size translates into a reduction in global cardiac mass. Factors present in the circulation of healthy mice are thus to some extent able to reverse critical structural and molecular aspects of cardiac aging. Although the full cast of factors involved in the rejuvenation of DCM are yet to be identified, our data provide proof of principle that signals from the systemic environment can override age-related, intrinsic changes in DCM, suggesting that these changes are predominantly epigenetic. In fact, in recent years, emerging evidence indicates that there are factors within the blood of young animals that have the ability to restore youthful characteristics to a number of organ systems in older animals[39,41]. These studies offer compelling evidence that effects of aged-associated disease can be reversed.

Risk assessment in DCM patients is currently limited to echocardiography studies, measurement of haemodynamic parameters and cardiopulmonary exercise performance. Understanding the role of epigenetic regulators in adult cardiac senescence provides a possible route towards more accurate profiling of cardiac dysfunction in dilated cardiomyopathies. Modulation of cardiac senescence response may further provide a novel strategy for treating heart failure, with Bmi1 serving as an attractive target.

**Figure 6 | Bmi1-mediated cardiomyocyte senescence. (a)** Cytochemical staining of SA-β-gal activity and immunostaining of Caspase 3 in paraffin sections of hearts from 15-week-old $Bmi1^{f/f};\alpha MHC\text{-}Cre^{tg/+}$ mice and $Bmi1^{f/}$ controls. Bars, 50 µm. **(b)** qRT–PCR analysis of $Bmi1$ mRNA expression in sorted populations of CMs, endothelial cells (ECs) and FBs from $Bmi1^{f/f};\alpha MHC\text{-}Cre^{tg/+}$ and $Bmi1^{f/}$ mice. Expression is standardized to β-actin and is expressed relative to the level in $Bmi1^{f/}$ mice (means ± s.d.; $n=12$, *$P<0.05$; Student's $t$-test). **(c)** Proliferation rate of CM, EC and FB subpopulations measured by *in vivo* BrdU incorporation over 1 week. Values are means ± s.d. ($n=5$). **(d,e)** Representative histograms for $C_{12}$-fluorescein show the relative levels of SA-β-gal in CM, EC and FB subsets from $Bmi1^{f};\alpha MHCCre$ and control mice (**d**); the values above the peaks are the median fluorescence intensities of the respective populations. **(e)** Percentage of SA-β-gal-positive cells in CM, EC and FB subpopulations. Values are means ± s.d. ($n=6$, *$P<0.05$; Student's $t$-test). **(f)** qRT–PCR analysis of the expression of $Bmi1$, $p16^{INK4a}$, $Ezh2$, $Myh7$, $Tgfβ$, $p53$ and $p21$ mRNA in total heart cells from $Bmi1^{fl/fl};\alpha MHC\text{-}Cre^{tg/+};p16^{INK4a-/-}$ mice and $Bmi1^{fl/fl};\alpha MHC\text{-}Cre^{+/+};p16^{INK4a-/-}$ mice. Values are means ± s.d.; $n=10$ (**$P<0.001$, *$P<0.05$; Student's $t$-test). **(g)** The gross cardiac phenotype of 12-week-old $Bmi1^{fl/fl};\alpha MHC\text{-}Cre^{+/+};p16^{INK4a-/-}$ ($Bmi1^{fl};p16^{-/-}$), $Bmi1^{fl/fl};\alpha MHC\text{-}Cre^{tg/+};p16^{INK4a+/+}$ ($Bmi1^{fl};\alpha MHCCre$) and $Bmi1^{fl/fl};\alpha MHC\text{-}Cre^{tg/+};p16^{INK4a-/-}$ ($Bmi1^{fl};\alpha MHCCre;p16^{-/-}$) mice. Representative views are shown of H&E-stained heart cross-sections at the midventricle (bars, 1 mm), Masson's trichrome staining of left ventricle to detect fibrosis (bars, 40 µm) and WGA staining to outline cardiomyocytes (bars, 10 µm). **(h–k)** HW/BW ratios (**h**), myocyte cross-sectional area (**i**), left ventricular wall thickness (**j**) and fractional shortening (**k**) in 12-week-old $Bmi1^{fl};p16^{-/-}$, $Bmi1^{fl};\alpha MHCCre$ and $Bmi1^{fl};\alpha MHCCre;p16^{-/-}$ mice. Data are means ± s.d. $n=8$ mice per group (*$P<0.05$; Student's $t$-test). **(l)** Cytochemical staining of SA-β-gal activity in paraffin sections of hearts from $Bmi1^{fl};p16^{-/-}$), $Bmi1^{fl};\alpha MHCCre$) and $Bmi1^{fl};\alpha MHCCre;p16^{-/-}$ mice. Scale bars, 50 µm. **(m,n)** Representative fluorescence histograms show the relative levels of SA-β-gal in CM, EC and FB subsets from $Bmi1^{fl};p16^{-/-}$ and $Bmi1^{fl};\alpha MHCCre;p16^{-/-}$ hearts (**m**); the values above the peaks are the median fluorescence intensities of the respective populations. Percentage of SA-β-gal-positive cells in CM, EC and FB subpopulations (**n**). Values are means ± s.d. ($n=6$; Student's $t$-test). **(o)** Kaplan–Meier survival curves for $Bmi1^{fl};p16^{-/-}$, $Bmi1^{fl};\alpha MHCCre$ and $Bmi1^{fl};\alpha MHC\text{-}Cre;p16^{-/-}$ littermates (means ± s.d., **$P<0.001$; Student's $t$-test).
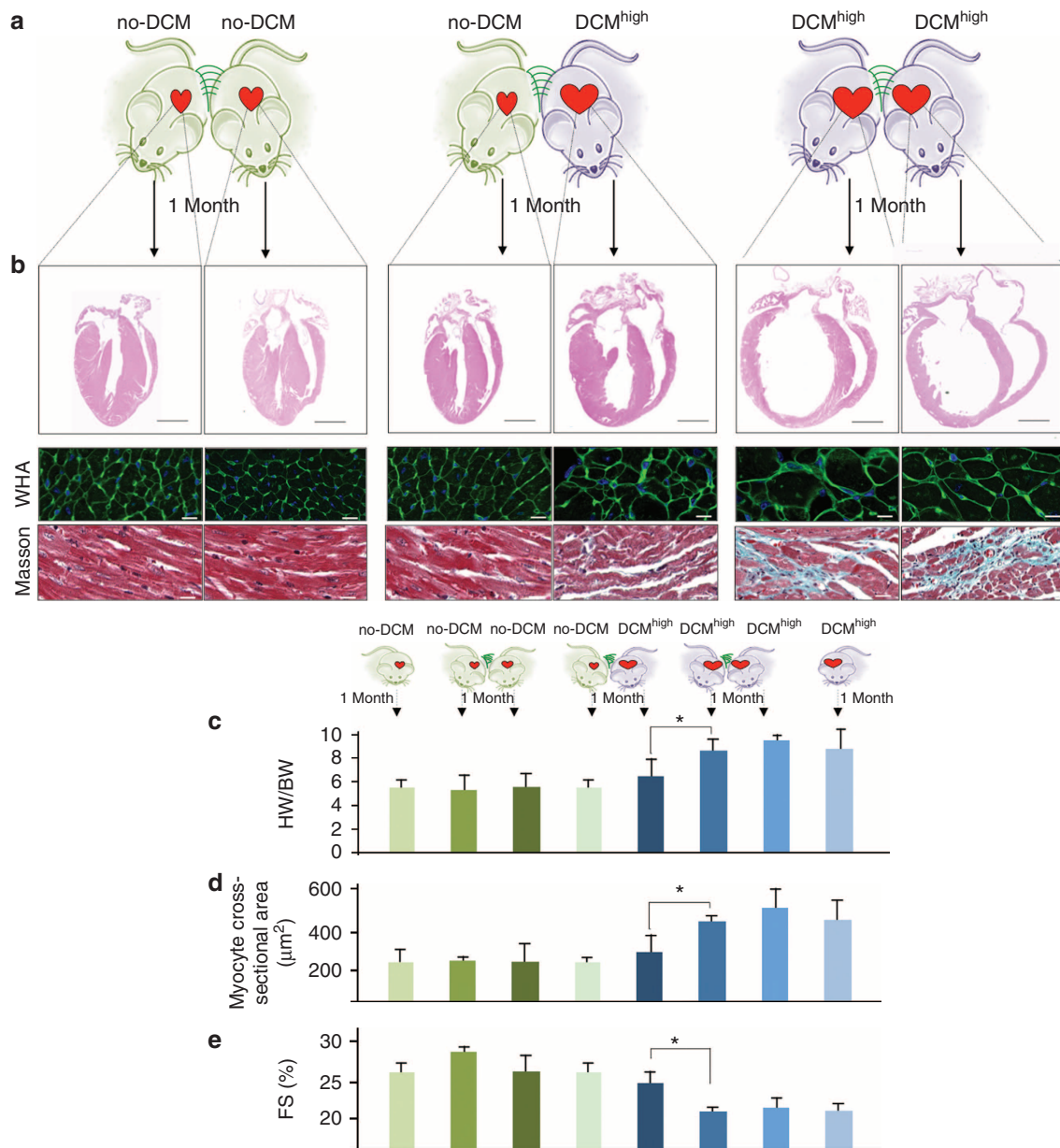
**Figure 7 | Paracrine senescence response of Bmi1-related DCM does not transmit to healthy mice.** (**a**) Parabiotic pairings; no-DCM as *Bmi1*$^{fl}$ mice and DCM$^{high}$ as *Bmi1*$^{fl/fl}$;*αMHC-Cre* mice. Comparisons were always made with littermate pairs (no-DCM to no-DCM or DCM$^{high}$ to DCM$^{high}$). (**b**) The gross cardiac phenotype of 12-week-old mice after 4 weeks of parabiosis as indicated. Representative views are shown of H&E-stained cross-sections at the midventricle (bars, 1 mm), Masson's trichrome staining of left ventricle to detect fibrosis (bars, 40 μm), and WGA staining to outline cardiomyocytes (bars, 10 μm). (**c–e**) HW/BW ratio (**c**), myocyte cross-sectional area (**d**) and fractional shortening (**e**) after 4 weeks of parabiosis as indicated. Data are means ± s.d.; $n = 8$ mice per group (*$P < 0.05$; Student's *t*-test).

## Methods

**Mice.** *ckoBmi1*$^{fl/+}$ mice[24] were backcrossed to the C57BL/6 background. Mice used in this study included *αMHC-Cre*$^{tg/+}$ (ref. 26), *αMHC*$^{TM}$*-Cre*$^{tg/+}$ (ref. 27), *Nkx2.5-Cre*$^{tg/+}$ (ref. 25), *MLC2-rRTA*$^{tg/+}$ (ref. 28) and *p16*$^{INK4a}$ $^{-/-}$ (ref. 38). The *αMHC-Cre*$^{tg/+}$ and *αMHC*$^{TM}$*-Cre*$^{tg/+}$ lines were kindly provided by Dr Redondo, *Nkx2.5-Cre*$^{tg/+}$ by Dr de la Pompa, *MLC2-rRTA*$^{tg/+}$ by Dr Lara-Pezzi and *p16*$^{INK4a}$ $^{-/-}$ by Dr Berns. For the generation of *tetO-Bmi1*$^{tg/+}$ mice, *Bmi1* cDNA was cloned into the pBS31 vector that included the minimal tetracycline-independent promoter. This Bmi1 vector was coelectroporated together with the vector harbouring FLPe recombinase under the control of the CAGGS promoter into KH2 ES cells (Open Biosystems). All genotyping primers are listed in Supplementary Table 1. All strains were on the C57BL/6J background; male and female mice aged 5–12 weeks were used, in the cases of not indicated. For *iBmi1*$^{tg/tg}$;*MLC2*$^{tg/+}$ and control mice, doxycycline (2 mg ml$^{-1}$, supplemented with sucrose at 5 mg ml$^{-1}$) was administered to mice in drinking water for 2 weeks). The *αMHC*$^{TM}$*-Cre* line and their control littermates were injected with 1 mg TM (Sigma) in corn coil on five consecutive days. All mice were bred in-house in a pathogen-free environment and were provided with standard care and nutrition according to the EU guidelines. All animal study proposals were approved by the Centro Nacional de Investigaciones Cardiovasculares (CNIC). For cardiogenesis studies, hearts at various embryonic stages or post-natal (P) days were collected for RNA/protein analysis or for histology.

**Echocardiography and MRI.** Echocardiograms were performed on mice anaesthetized with 2.0% isoflurane, using a Vevo 770 High-Resolution *In Vivo* Micro-Imaging System and RMV 707B Scanhead (VisualSonics Inc). Scans were conducted by two experienced researchers blinded to the mouse genotype. Measurements of left parasternal long and short axes and M-mode (left parasternal short axis) images were obtained at a heart rate of 500–550 bpm. LV end-diastolic diameter (LVEDD), LV end-systolic diameter (LVESD) and wall thickness were measured from M-mode tracings, and the average of three consecutive cardiac cycles is reported. The LV fractional shortening percentage was calculated as
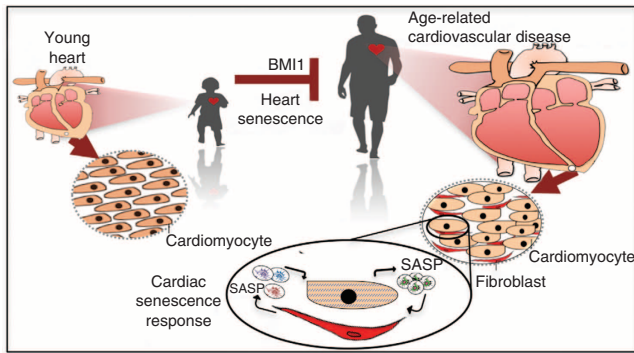
**Figure 8 | A model for the impact of cardiac-specific Bmi1 action. (a)** As aging poses the largest risk for cardiovascular disease, the cardiac Bmi1 action could be determinant to limit the heart senescence response. Our data establish the idea that the nonproliferative cardiomyocyte-related senescence phenotype can be locally propagated through the SASP.

$([LVEDD - LVESD]/LVEDD) \times 100$ MRI of lung was performed with a 7-T Agilent scanner (Agilent, Santa Clara, USA) equipped with a DD2 console and an actively shielded gradient set (205/120 insert of maximum $130\,mT\,m^{-1}$ gradient strength). For image acquisition, we employed a combination of volume coil/surface coil coil to enhance signal-to-noise ratio formed by a 72-mm inner diameter quadrature birdcage TX coil (Rapid Biomedical GmBH, Germany) and an actively detuning 30-mm flexible customized surface RX coil (Neos Biotec, Pamplona, Spain). Following a tripilot gradient-echo image, a gradient-echo sequence without gating was used to acquire oblique coronal slices (one to two slices) and axial slices (7–10 slices covering the entire lung, 72-s acquisition time per slice) using the following parameters: TR/TE = 6.7/2.2 ms, flip angle = 10 degree, bandwidth = 100 kHz, field of view = $3 \times 3$ cm, matrix = $256 \times 128$, slice thickness = 1 mm and number average experiment (Number average EXperiments = 60). Mice were anaesthetized with 2% isoflurane and oxygen and positioned on a thermoregulated (38.7 °C) mouse bed. Ophthalmic gel was placed in their eyes to prevent retinal drying.

**Human DCM samples.** The study population comprised six patients with medically refractory DCM, excluding specifically those patients with the evidence of ischaemic cardiomyopathy or myocarditis. Before cardiac transplantation, patients received a two-stage drug regime designed to avoid deterioration (β1/β2-blocker (carvedilol), angiotensin-converting enzyme inhibitor (lisinopril), angiotensin receptor I antagonist (losartan) and aldosterone antagonist (spironolactone)). Patients were subsequently switched to a selective β1 blocker (bisoprolol) and given the β2-agonist, clenbuterol, with a view to stimulate hypertrophy and improve cardiac function. Echocardiography and exercise testing were performed regularly during treatment before transplantation to monitor the recovery process. In addition, four ventricular samples were available for mRNA analysis from donor organs used for transplantation ($n = 2$), and donor organs unsuitable for transplantation ($n = 2$). Data collected from these RNA samples were used in gene expression analyses.

**Histology and immunohistochemical analyses.** For histological analysis, embryos or heart tissues were fixed in 10% paraformaldehyde (PFA) at the stages indicated in each figure legend, dehydrated and embedded in paraffin for preparation of 5- or 10-μm histological sections. Rehydrated slides were stained with haematoxylin and eosin and Masson's trichrome. For determination of CM cross-sectional area, deparaffinized and rehydrated heart sections were incubated for 1 h at room temperature with fluorescein isothiocyanate (FITC)-labelled wheatgerm agglutinin (Sigma-Aldrich) to visualize myocyte membranes. Regions that included the circular shapes of capillaries were selected from the epicardial side of the LV-free walls. The mean cross-sectional area of CMs was determined from 60 to 80 cells. For fluorescence detection of SA-β-gal activity, cells ($10^7$ cell ml$^{-1}$) were incubated with $C_{12}FDG$ (fluorescein di-β-D-galactopyranoside; 33 μM; Sigma), a β-galactosidase substrate that generates a fluorescent product upon cleavage, for 60 min at 37 °C (ref. 35). Cytochemical detection of senescent cells *in vitro* was determined in cells and fixed tissues with the Senescence β-Galactosidase Staining Kit (Cell Signaling).

**Chromatin immunoprecipitation (ChIP) assays.** For ChIP analysis, we used sorted $10^6$ cells per condition and added formaldehyde directly to the tissue culture medium to a final concentration of 1% and incubated cultures for 10 min at room temperature on a shaking platform. We stopped the crosslinking by adding glycine to a final concentration of 0.125 M. We washed crosslinked cells twice with cold phosphate-buffered saline and lysed them at a density of $5 \times 10^6$ cells ml$^{-1}$ for 10 min at 4 °C in 1% SDS, 50 mM Tris-HCl (pH 8.0) and 10 mM EDTA-containing protease inhibitors. We sonicated lysates to obtain chromatin fragments <1 kb and

centrifuged them for 15 min in a microfuge at room temperature. We diluted 400 μl of lysate 1:10 with 1.1% Triton-X100, 2 mM EDTA, 150 mM NaCl and 20 mM Tris-HCl (pH 8.0) containing protease inhibitors, precleared with 50% salmon sperm DNA and protein A agarose slurry (Upstate). Antibodies used for ChIP assays[42] were rabbit polyclonal anti-Bmi1, H3K27me3, H2AK119 and H3K4me3 (all from Upstate; 1:2,500). We then added salmon sperm DNA and protein A agarose beads (60 μl) and incubated for 1 h. We washed the immunoprecipitated pellets with 0.1% SDS, 1% Triton-X100, 2 mM EDTA, 20 mM Tris-HCl (pH 8.0) and 150 mM NaCl (one wash); 0.1% SDS, 1% Triton-X100, 2 mM EDTA, 20 mM Tris-HCl (pH 8.0) and 500 mM NaCl (one wash); 0.25 M LiCl, 1% Nonidet P-40, 1% sodium deoxycholate, 1 mM EDTA and 10 mM Tris-HCl, pH 8.0 (one wash); and 10 mM Tris-HCl (pH 8.0) and 1 mM EDTA (two washes). We then eluted the chromatin from the beads twice by incubation with 250 μl 1% SDS and 0.1 M NaHCO₃ during 15 min at room temperature with rotation. After adding 20 μl of 5 M NaCl, we reversed the crosslinks for 4 h at 65 °C. Samples were supplemented with 20 μl of 1 M Tris-HCl (pH 6.5), 10 μl of 0.5 M EDTA, 20 μg of RNase A and 40 μg of proteinase K and incubated for 1 h at 45 °C. DNA from precipitated complexes was amplified using reverse transcription–polymerase chain reaction (RT–PCR). RT–PCR amplifications were performed in triplicate with multiple dilutions, and primer sequences are included in the Supplementary Table 1.

**RNA extraction and real-time PCR.** Heart tissue samples were stored in RNAlater RNA stabilization reagent (QIAGEN) at 4 °C. Total RNA was extracted using the RNeasy Fibrous Tissue Mini Kit (QIAGEN). First-strand cDNA synthesis was performed with 1 μg of total RNA, random hexamers and SuperScript III Reverse Transcriptase (Invitrogen). Real-time PCR was performed using a QuantiTect SYBR Green PCR kit (QIAGEN) in a Light-Cycler (Roche). The expression level of each gene was normalized to that of 18S rRNA, which served as an endogenous internal control. The primer sequences are available at the Supplementary Table 1.

**Cardiac hypertrophy induction.** Isoproterenol (60 mg per kg body weight) was administered to 9-week-old mice for 14 days using subdermally implanted ALZET osmotic minipumps. PBS-filled minipumps were used as a control. For TAC surgery, mice (8–10 weeks old, 21–24 g body weight) were anaesthetized by intraperitoneal injection of a mixture of xylazine (5 mg kg$^{-1}$) and ketamine (100 mg kg$^{-1}$). The animals were then placed in a supine position, an endotracheal tube was inserted and the animals were ventilated using a volume-cycled rodent ventilator with a tidal volume of 0.4 ml room air and a respiratory rate of 110 breaths per minute. The chest cavity was exposed by cutting open the proximal portion of the sternum. The aortic arch between the innominate and left common carotid arteries was isolated and was constricted with a 7–0 nylon suture tied firmly three times against a 25-gauge blunted needle for LI-TAC or a 27-gauge needle for HI-TAC. Sham-operated mice underwent the same surgical procedure, including isolation of the aorta, but without placement of the suture.

**Tgf-β blocking activity assay.** DCM mice ($Bmi1^{fl}\alpha MHC\text{-}Cre^{tg/+}$) received intraperitoneal injections of Tgf-β antibody (10 mg per kg body weight in PBS; AB-100-NA; R&D Systems) every 3 days for 2 weeks before being killed. Control mice were treated with identical doses of rabbit IgG (R&D Systems).

**Protein analysis.** Antibodies used for western blots were as follows: anti-Bmi1 (Millipore), anti-Ezh2 (Active Motif), anti-aMHC (Millipore), anti-H3K9me3 (Upstate), anti-murine p16 (Santa Cruz Biotechnology), anti-human p16 (Cell Signaling) and anti-β-actin (Sigma; these antibodies were used at 1:500). Secondary antibody was the horseradish peroxidase-linked anti-mouse IgG (Dako; 1:2,500).

**Isolation of CMs and cardiac FBs.** Cells were isolated from Langendorff heart preparations followed by enzymatic digestion[43]. For isolation of nonmyocyte-enriched cells, hearts were dissected free of vessels and atria, washed in ice-cold modified Krebs–Henseleit bicarbonate buffer (pH 7.2; Sigma-Aldrich) and rapidly cut into pieces. The heart pieces were incubated in 5 ml of digesting solution (0.25 mg ml$^{-1}$ Liberase TH (Roche) and 10 mM HEPES in balanced salt solution-containing calcium and magnesium) for 8 min at 37 °C with vigorous stirring. The supernatant was then added to 10 ml of ice-cold Krebs–Henseleit bicarbonate. Five millilitres of fresh digesting solution were added to the remaining tissue fragments, and the digestion and sampling steps were repeated until all the tissues were dissolved. The collected cells were filtered through a 35-μm nylon mesh (BD Falcon) and then used for flow cytometry. Different cellular subsets were incubated with phycoerythrin-conjugated anti-Thy1 antibody (eBioscience), FITC-conjugated anti-CD31 antibody (BD Biosciences) and allophycocyanin-conjugated CD3 antibody (eBioscience), after which they were analysed and sorted on a FACSAria II flow cytometer (BD Biosciences) using the FlowJo softwarem (these antibodies were used at 1:100). For analysis of SA-β-gal expression, cells were incubated with the fluorogenic β-galactosidase substrate fluorescein di-β-D-galactopyranoside (1:250).

**Cell proliferation.** BrdU (Sigma-Aldrich) was injected daily into the peritoneum (100 mg per kg body weight in PBS) for 3 days, with the last injection 2 h before

harvesting the hearts. The hearts were fixed in 4% PFA, paraffin-embedded and sectioned. BrdU-positive nuclei were detected with mouse monoclonal anti-BrdU primary antibody (Dako; 1:250) and immunofluorescent staining as described above. BrdU- or Ki67-labelled cells and 4′,6-diamidino-2-phenylindole (DAPI)-stained nuclei were counted in nonmyocyte cells from 5 to 10 fields ( × 400 magnification) with focal fibrosis and/or expanded interstitium (identified with wheatgerm agglutinin staining) and in areas with preserved myocardial architecture (for example, absence of both focal fibrosis and expanded interstitium) in 9–15 sections per heart. Myocytes were identified with fluorescent microscopy visualization of sarcomeres. Nuclei of sarcomere-negative cells within interstitial regions were designated as nonmyocyte nuclei. Nuclei were quantified using the ImageJ nucleus counter software. The percentage of proliferating cells was calculated as the number of positive BrdU- or Ki67-labelled nuclei divided by the number of DAPI-stained nuclei.

**Parabiosis.** Anaesthetized mice were shaved at the corresponding lateral aspects and matching skin incisions were made from the olecranon to the knee joint of each mouse, and the subcutaneous fascia was bluntly dissected to create ∼0.5 cm of free skin. The olecranon and knee joints were attached by a single 5–0 polypropylene suture and tie, and the dorsal and ventral skins were approximated by continuous suture. A single dose of flunixin meglumine (Schering-Plough, $1 \, mg \, kg^{-1}$) was injected subcutaneously into each partner at the end of the surgical procedure. One month after surgery, blood samples were obtained from each of the partners for analysis of haematopoietic progenitors.

**Statistical analysis.** All data are expressed as the mean ± s.d. Paired data were evaluated using Student's $t$-test. Survival rates among mice were analysed using the long-rank test. Differences were considered statistically significant at $P < 0.05$.

## References

1. McNally, E. M., Golbus, J. R. & Puckelwartz, M. J. Genetic mutations and mechanisms in dilated cardiomyopathy. *J. Clin. Invest.* **123,** 19–26 (2013).
2. Harvey, P. A. & Leinwand, L. A. The cell biology of disease: cellular mechanisms of cardiomyopathy. *J. Cell Biol.* **194,** 355–365 (2011).
3. Sauvageau, M. & Sauvageau, G. Polycomb group proteins: multi-faceted regulators of somatic stem cells and cancer. *Cell Stem Cell* **7,** 299–313 (2010).
4. Dobreva, G. & Braun, T. When silence is broken: polycomb group proteins in heart development. *Circ. Res.* **110,** 372–374 (2012).
5. Chang, C. P. & Bruneau, B. G. Epigenetics and cardiovascular development. *Annu. Rev. Physiol.* **74,** 41–68 (2012).
6. Hang, C. T. *et al.* Chromatin regulation by Brg1 underlies heart muscle development and disease. *Nature* **466,** 62–67 (2010).
7. Delgado-Olguin, P. *et al.* Epigenetic repression of cardiac progenitor gene expression by Ezh2 is required for postnatal cardiac homeostasis. *Nat. Genet.* **44,** 343–347 (2012).
8. Ng, S. B. *et al.* Exome sequencing identifies MLL2 mutations as a cause of Kabuki syndrome. *Nat. Genet.* **42,** 790–793 (2010).
9. Ieda, M. *et al.* Direct reprogramming of fibroblasts into functional cardiomyocytes by defined factors. *Cell* **142,** 375–386 (2010).
10. Wamstad, J. A. *et al.* Dynamic and coordinated epigenetic regulation of developmental transitions in the cardiac lineage. *Cell* **151,** 206–220 (2012).
11. Bracken, A. P. & Helin, K. Polycomb group proteins: navigators of lineage pathways led astray in cancer. *Nat. Rev. Cancer* **9,** 773–784 (2009).
12. Salama, R., Sadaie, M., Hoare, M. & Narita, M. Cellular senescence and its effector programs. *Genes Dev.* **28,** 99–114 (2014).
13. Krizhanovsky, V. *et al.* Senescence of activated stellate cells limits liver fibrosis. *Cell* **134,** 657–667 (2008).
14. Narita, M. *et al.* Rb-mediated heterochromatin formation and silencing of E2F target genes during cellular senescence. *Cell* **113,** 703–716 (2003).
15. Collado, M., Blasco, M. A. & Serrano, M. Cellular senescence in cancer and aging. *Cell* **130,** 223–233 (2007).
16. Kuilman, T., Michaloglou, C., Mooi, W. J. & Peeper, D. S. The essence of senescence. *Genes Dev.* **24,** 2463–2479 (2010).
17. Acosta, J. C. *et al.* A complex secretory program orchestrated by the inflammasome controls paracrine senescence. *Nat. Cell Biol.* **15,** 978–990 (2013).
18. Di Croce, L. & Helin, K. Transcriptional regulation by Polycomb group proteins. *Nat. Struct. Mol. Biol.* **20,** 1147–1155 (2013).
19. Jacobs, J. J., Kieboom, K., Marino, S., DePinho, R. A. & van Lohuizen, M. The oncogene and Polycomb-group gene bmi-1 regulates cell proliferation and senescence through the ink4a locus. *Nature* **397,** 164–168 (1999).
20. Bruggeman, S. W. *et al.* Ink4a and Arf differentially affect cell proliferation and neural stem cell self-renewal in Bmi1-deficient mice. *Genes Dev.* **19,** 1438–1443 (2005).
21. Molofsky, A. V. *et al.* Increasing p16INK4a expression decreases forebrain progenitors and neurogenesis during ageing. *Nature* **443,** 448–452 (2006).
22. Oguro, H. *et al.* Differential impact of Ink4a and Arf on hematopoietic stem cells and their bone marrow microenvironment in Bmi1-deficient mice. *J. Exp. Med.* **203,** 2247–2253 (2006).
23. Akala, O. O. *et al.* Long-term haematopoietic reconstitution by Trp53-/- p16Ink4a-/-p19Arf-/- multipotent progenitors. *Nature* **453,** 228–232 (2008).
24. Arranz, L. *et al.* Bmi1 is critical to prevent Ikaros-mediated lymphoid priming in hematopoietic stem cells. *Cell Cycle* **11,** 65–78 (2012).
25. Moses, K. A., DeMayo, F., Braun, R. M., Reecy, J. L. & Schwartz, R. J. Embryonic expression of an Nkx2-5/Cre gene using ROSA26 reporter mice. *Genesis* **31,** 176–180 (2001).
26. Agah, R. *et al.* Gene recombination in postmitotic cells. Targeted expression of Cre recombinase provokes cardiac-restricted, site-specific rearrangement in adult ventricular muscle *in vivo*. *J. Clin. Invest.* **100,** 169–179 (1997).
27. Sohal, D. S. *et al.* Temporally regulated and tissue-specific gene manipulations in the adult and embryonic heart using a tamoxifen-inducible Cre protein. *Circ. Res.* **89,** 20–25 (2001).
28. Breckenridge, R. A. *et al.* Overexpression of the transcription factor Hand1 causes predisposition towards arrhythmia in mice. *J. Mol. Cell Cardiol.* **47,** 133–141 (2009).
29. North, B. J. & Sinclair, D. A. The intersection between aging and cardiovascular disease. *Circ. Res.* **110,** 1097–1108 (2012).
30. Hidalgo, I. *et al.* Ezh1 is required for hematopoietic stem cell maintenance and prevents senescence-like cell cycle arrest. *Cell Stem Cell* **11,** 649–662 (2012).
31. Lowe, S. W., Cepero, E. & Evan, G. Intrinsic tumour suppression. *Nature* **432,** 307–315 (2004).
32. Coppe, J. P., Desprez, P. Y., Krtolica, A. & Campisi, J. The senescence-associated secretory phenotype: the dark side of tumor suppression. *Annu. Rev. Pathol.* **5,** 99–118 (2010).
33. Agherbi, H. *et al.* Polycomb mediated epigenetic silencing and replication timing at the INK4a/ARF locus during senescence. *PLoS ONE* **4,** e5622 (2009).
34. Gonzalez, S. *et al.* Oncogenic activity of Cdc6 through repression of the INK4/ ARF locus. *Nature* **440,** 702–706 (2006).
35. Debacq-Chainiaux, F., Erusalimsky, J. D., Campisi, J. & Toussaint, O. Protocols to detect senescence-associated beta-galactosidase (SA-betagal) activity, a biomarker of senescent cells in culture and *in vivo*. *Nat. Protoc.* **4,** 1798–1806 (2009).
36. Shioya, T. A simple technique for isolating healthy heart cells from mouse models. *J. Physiol. Sci.* **57,** 327–335 (2007).
37. Takeda, N. *et al.* Cardiac fibroblasts are essential for the adaptive response of the murine heart to pressure overload. *J. Clin. Invest.* **120,** 254–265 (2010).
38. Krimpenfort, P. *et al.* p15Ink4b is a critical tumour suppressor in the absence of p16Ink4a. *Nature* **448,** 943–946 (2007).
39. Loffredo, F. S. *et al.* Growth differentiation factor 11 is a circulating factor that reverses age-related cardiac hypertrophy. *Cell* **153,** 828–839 (2013).
40. Campisi, J. Cellular senescence: putting the paradoxes in perspective. *Curr. Opin. Genet. Dev.* **21,** 107–112 (2011).
41. Addis, R. C. & Epstein, J. A. Induced regeneration--the progress and promise of direct reprogramming for heart repair. *Nat. Med.* **19,** 829–836 (2013).
42. Gonzalez, S., Pisano, D. G. & Serrano, M. Mechanistic principles of chromatin remodeling guided by siRNAs and miRNAs. *Cell Cycle* **7,** 2601–2608 (2008).
43. Schmitt, J. P. *et al.* Dilated cardiomyopathy and heart failure caused by a mutation in phospholamban. *Science* **299,** 1410–1413 (2003).

## Author contributions

I.G.-V. has performed most of the experiments; I.H., L.P.-B., P.G., J.M.R. and A.B. have contributed to data analysis and discussion of the paper; J.M.R.-C., L.J.J.-B. have performed the imaging data; P.G.-P. and E.L.-P. have contributed with the samples of DCM patients; J.A.E., J.L.d.l.P. and A.H. have supervised the data analysis; S.G. designed and supervised the study and wrote the paper.

## Additional information

**Accession codes**: The RNAseq data from mDCM and hDCM samples have been deposited in the Gene Expression Omnibus under accession code GSE64391 and GSE65447, respectively

**Supplementary Information** accompanies this paper at http://www.nature.com/naturecommunications

**Competing financial interests:** The authors declare no competing financial interests.

**Reprints and permission** information is available online at http://npg.nature.com/reprintsandpermissions/

**How to cite this article:** Gonzalez-Valdes, I. *et al.* Bmi1 limits dilated cardiomyopathy and heart failure by inhibiting cardiac senescence. *Nat. Commun.* 6:6473 doi: 10.1038/ncomms7473 (2015).

# Retraction: Bmi1 limits dilated cardiomyopathy and heart failure by inhibiting cardiac senescence

I. Gonzalez-Valdes, I. Hidalgo, A. Bujarrabal, E. Lara-Pezzi, L. Padron-Barthe, P. Garcia-Pavia,
Pablo Gómez-del Arco, J.M. Redondo, J.M. Ruiz-Cabello, L.J. Jimenez-Borreguero, J.A. Enriquez,
J.L. de la Pompa, A. Hidalgo & S. Gonzalez

We the authors are retracting this Article as it has come to our attention that there has been inappropriate duplication of images between different figures of the published paper, and between figures in the paper and those in work previously published by the corresponding author (Hidalgo, I. *et al.* 2012). The figure panels affected are Figure 1d, Figure 3c, Figure 4e, Figures 6a, g, and Supplementary Figure 1b. The corresponding author, S. Gonzalez, was unable to supply a complete set of raw data on which the Article is based. The Centro Nacional de Investigaciones Cardiovasculares Carlos III and the first author I. Gonzalez-Valdes, together with the co-authors I. Hidalgo, A. Bujarrabal, E. Lara-Pezzi, L. Padron-Barthe, P. Garcia-Pavia, Pablo Gómez-del Arco, J.M. Redondo, J.M. Ruiz-Cabello, L.J. Jimenez-Borreguero, J.A. Enriquez, J.L. de la Pompa, and A. Hidalgo, agree with retraction of the Article.

Hidalgo, I. *et al.* Ezh1 is required for hematopoietic stem cell maintenance and prevents senescence-like cell cycle arrest. *Cell Stem Cell* **11**, 649–662 (2012).